Transactions of the SMiRT 27
Yokohama, Japan, March 3-8, 2024
Division I

UNDERSTAND NANO-INDENTATION RESULTS BY ANALYSIS OF MICROSCALE DEFECTS UNDER DIFFERENT CONDITIONS OF HEAVY ION IRRADIATION

Dongyue CHEN[*, 1], Kenta MURAKAMI[2], Shasha LV[3], Zhengcao LI[1], Naoto SEKIMURA[2]

[1] Tsinghua University, Beijing, China
[2] The University of Tokyo, Tokyo, Japan
[3] Beijing Normal University, Beijing, China
[*] Associate Professor (dychen@tsinghua.edu.cn)

ABSTRACT

The ageing evaluation of stainless steel components in light water reactors largely relies on the experimental databases of mechanical properties. Still, continuous efforts are desired to understand the evolution of microscopic defects, which are the origin of the mechanical degradation. In this study, the effects of Si content and irradiation temperature on the irradiation hardening of stainless steel were investigated and explained by microstructural analysis. It was found that irradiation hardening was lower at 400 °C compared to 350 °C and 450 °C when irradiated to 5 dpa, and the hardening increased as Si content increased from 0.42 to 0.95 wt.%. The irradiation hardening was determined by the number density and size of Frank loops at 350 °C; however, at 450 °C, loop unfaulting was obvious and the contribution of Ni-Si clusters also needs to be considered.

INTRODUCTION

Stainless steel is the major structural material in light water reactors. It's used as plates, barrels, baffles, formers, bolts, and so on in the reactor core region. The integrity and function of stainless steel components are challenged by the working environment of high temperature and high irradiation dose [1], which leads to hardening [2, 3], embrittlement, and irradiation assisted stress corrosion cracking [4]. The safety standards to evaluate stainless steel component ageing in light water reactors largely rely on the experimental databases of mechanical properties [5, 6]. Although it is straightforward and practical to carry out standards based on macroscopic mechanical properties, continuous efforts are desired to trace back to the microscopic defects, which are the origin of the mechanical degradation.

Irradiation hardening is a typical and important mechanical degradation for stainless steel in light water reactors. It is closely related to the nucleation and growth of micro-defects, namely, black dots, Frank loops, perfect loops, Ni-Si clusters, and cavities [7]. The relationship between micro-defects and irradiation hardening is quantitatively described by the Orowan model [8, 9]. Frank loop is a key contributor to irradiation hardening in stainless steel, and the evolution of Frank loops under irradiation is a complicated process that highly depends on the Si content of the alloy and irradiation temperature [10, 11]. When the irradiation temperature is high, Frank loops may unfault into perfect loops [12]. Si content may influence the density and size of Frank loops. Shigenaka et al. found the addition of 0.30 wt.% Si promoted the number density of dislocation loops at several temperatures, but further addition of 2.52 wt.% Mo canceled the loop density promotion [13]. Fukuya et al. also found Si addition to enhance loop nucleation [14]. However, Miwa et al. found loop density was suppressed by Si addition [15].

In this study, model alloys of stainless steel with different Si content were irradiated to 5 dpa at different temperatures. The irradiation hardening under different conditions was measured and compared with microstructural analysis. The effects of Si content and irradiation temperature on dislocation loop formation were investigated.

METHODOLOGY

Model Alloys

Two types of model alloys were used: the BA (Base Si) specimen and the HS (High Si) specimen. The composition of the BA specimen was Fe-17.3Cr-13.2Ni-2.36Mo-0.88Mn-0.42Si in weight percentage, and the composition of the HS specimen was Fe-17.0Cr-13.5Ni-2.27Mo-0.99Mn-0.95Si. Both alloys were the high-purity alloy of 316L stainless steel, and the major difference was the Si content. The model alloys were solution annealed at 1080°C for 0.5 hours to minimize pre-existing dislocations.

The bulk alloy was cut into small pieces of around 10×2×0.5mm in dimension. Paper polishing was finalized with 2400# SiO_2 emery paper, followed by buff polishing using 3 μm diamond solution and polishing cloth. To remove the possible mechanical damage layer left by paper polishing, electrochemical polishing was conducted using the electrolyte of 90% acetic acid and 10% perchloric acid in an ice-water bath. Then, the specimen surface was ready for nano-indentation and ion irradiation.

Heavily Ion Irradiation

The ion irradiation was performed in the High Fluence Irradiation Facility at Tokai campus of the University of Tokyo. The irradiation particle was 3 MeV Ni^{2+}. The damage profile was calculated by the SRIM-2013 code [16] with the displacement energy of 40 eV [17-19], and the result is shown in Figure 1. The irradiation dose was 5 dpa, defined by the arithmetic average between the top surface and the depth of damage peak. The dose rate was approximately ~3×10^{-4} dpa/s.

Irradiation temperature was 350, 400 and 450 °C. The temperature was controlled by the heater and water-cooling system and monitored by two thermal couples. During the irradiation, the temperature fluctuation in reading number was less than ±2°C, and the vacuum was kept at around ~1×10^{-5} Pa.

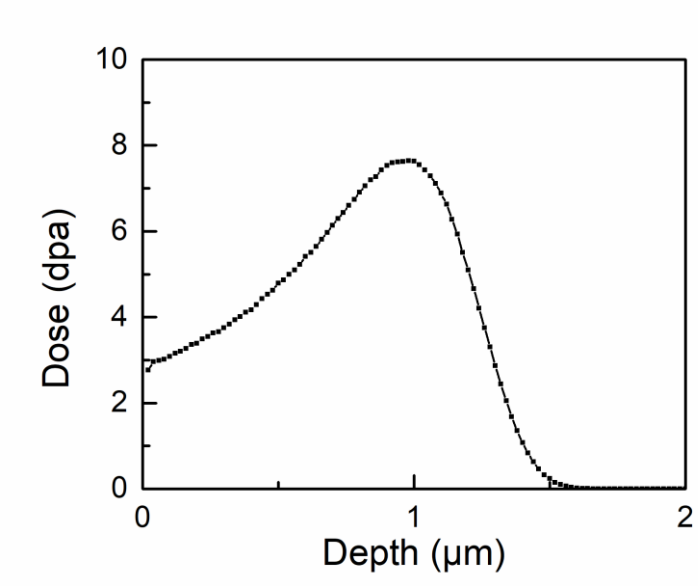

Figure 1. Damage profile of 3 MeV Ni^{2+} irradiation in stainless steel calculated by the SRIM-2013 code. The calculation was performed using the Kinchin-Pease model with a displacement energy of 40 eV.

Nano Indentation

Irradiation hardening was tested by nano-indentation following the ISO-14577 standard. The nano-indentation was performed using the Shimadzu DUH-211 with a Berkovich indenter. A constant indentation depth of 200 nm was kept for all the specimens.

For each specimen, 200 indents were indented before irradiation, and another 200 indents were indented after irradiation. The distance between two neighboring indents was as large as 30 μm, so the possible interactions between plastic zones could be minimized. The 200 indents covered a region of 600×300 μm on the sample surface, which was large enough to cover over ~50 grains. Consequently, the resultant nano-hardness was an average value of many grains with various orientations to minimize the possible influences from grain orientation [20]. After irradiation, the 600×300 μm indent array was performed in the region near the indent arrays tested before the irradiation.

Transmission Electron Microscopy

Transmission electron microscopy (TEM) specimens were prepared by the focused ion beam (FIB) technique. Hitachi FB-2100 was used as the FIB machine. The specimens were pre-thinned by FIB to approximately 200 nm thick and then further thinned by electrochemical polishing. The primary purpose of the electrochemical polishing was to remove the FIB damage on the surface of the thin foil. The electrochemical polishing was conducted for a very short period of time, usually around 0.01–0.1 sec. The electrolyte was 5% perchloric acid and 95% ethanol, and the polishing voltage was 40 V. As indicated in Figure 1, the region beyond 2 μm depth should be almost defect-free under TEM; otherwise, it means the FIB damage was not successfully removed by electrochemical polishing.

TEM observation was conducted using the JEM-2000FX under a voltage of 200 kV. The observation was carried out in the 800–1000 nm depth region, which covers the damage peak (Figure 1). Dark-field imaging was performed under the $\boldsymbol{g}$ vector of <200>. Relrod techniques were applied to identify Frank loops [21] by tilting the TEM foil ~7° off the <110> zone axis while maintaining the $\boldsymbol{g}$=<113> dynamic two-beam condition. TEM foil thickness was estimated under $\boldsymbol{g}$=<200> and $\boldsymbol{g}$=<111> by thickness fringes [22].

RESULTS AND DISCUSSION

Irradiation Hardening

The nano-indentation results before and after irradiation are shown in Figure 2. The data scattering of each 200 indents was in a reasonable range, and only few data points with irregular values were found. When the composition was fixed, the hardness difference between each unirradiated sample was minimal, supporting the reliability of our specimen preparation and indentation processes.

Generally, the increase in nano-harness after irradiation was evident for all the specimens. When the irradiation temperature was the same, the increment in hardness was larger in the HS specimens than that in the BA specimens. In the BA specimens, irradiation hardening was smaller in the case of 400 °C irradiation, and was larger in 350 °C irradiation and 450 °C irradiation. Similarly, the hardening was the smallest for the HS specimens at 400 °C compared to the other two irradiation temperatures.

In Figure 3, the irradiation hardening and the corresponding standard deviation were plotted as a function of alloy Si content. The results in our previous works were also added to the figure for comparison, including irradiation on non-Si alloy [23], irradiation at 400 °C to 3 dpa [24], and irradiation at 290 °C to 0.8 dpa [25].

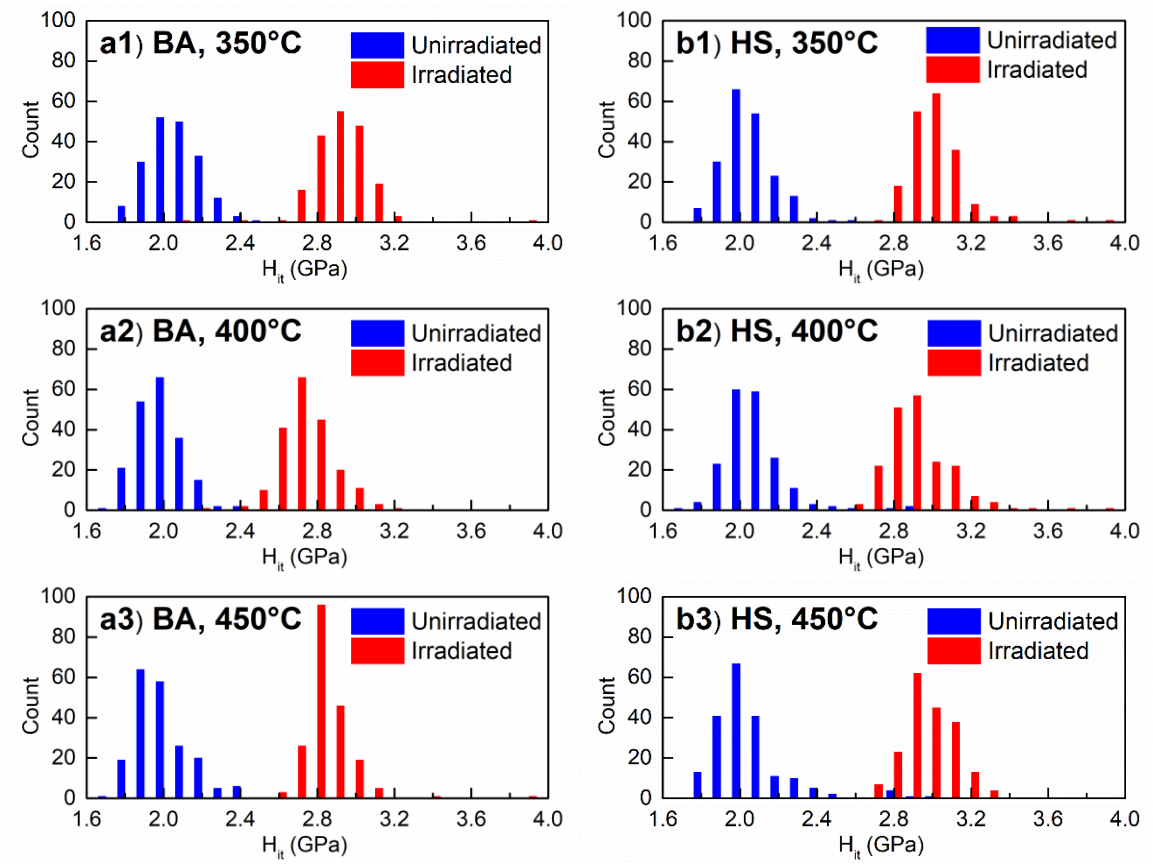

Figure 2. Distribution of nano-indentation results of a) BA and b) HS specimens before and after 5 dpa irradiation at different temperatures.

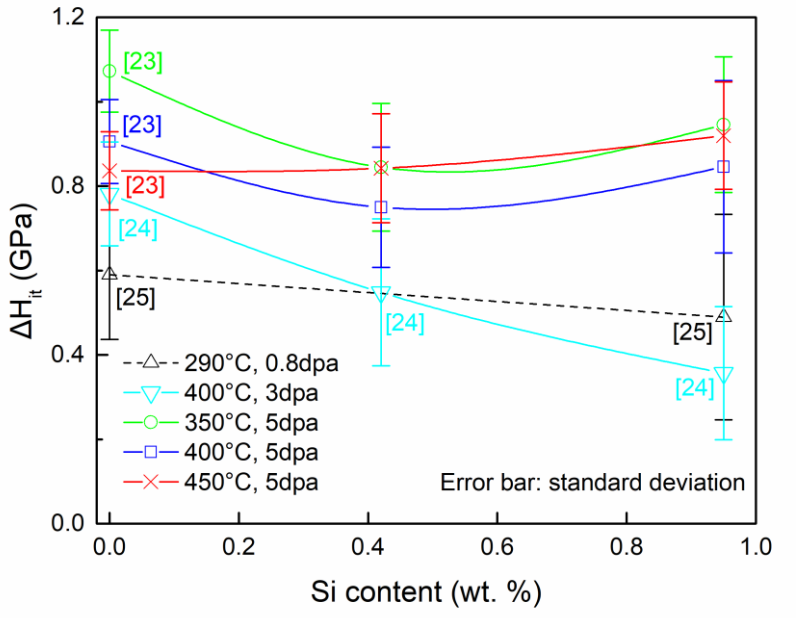

Figure 3. Irradiation hardening results tested by nano-indentation and compared with our previous results [23-25].

When irradiated to 3 dpa at 400 °C, irradiation hardening monotonically decreased as Si content increased [24]. As the irradiation dose reached 5 dpa at the same temperature, the amount of hardening

increased for all three compositions, but the curve was no longer monotonic. To be more precise, the irradiation hardening decreased as Si content increased from 0% to 0.42 wt.% but increased again when Si content reached 0.95 wt.%. A similar curve trend was also observed in 350 °C and 5 dpa irradiation, but the absolute value of hardening was even higher compared to the 400 °C and 5 dpa irradiation. The high value of hardening at 350 °C may have come from the higher density of defects at lower temperature. In 450 °C and 5 dpa irradiation, the hardening monotonically increased as a function of Si content, which was a unique trend compared to the 5 dpa irradiation at the other two temperatures. The changes in those hardening trends indicated the different roles of Si played in those irradiations with different temperature and dose.

Microscale Defects

Radiation defects were examined using TEM under 200 kV. Voids were not discovered in all the specimens, so dislocation loops were analyzed in detail. It is effective to separate Frank loops and perfect loops by comparing dark-field and relrod images [26]. In a dark-field image using ***g***=<200>, 100% of Frank loops and 2/3 of perfect loops are visualized. In a relrod image, 1/4 of Frank loops can be seen theoretically, as Frank loops have four variants of {111} stacking faults. But we need to be careful whether Frank loops follow the isotropic distribution or not [27]. In stainless steel irradiated at 500 °C, Liu et al. reported the distribution of Frank loops was isotropic at 10 dpa but anisotropic at 50 and 150 dpa [28]. As our irradiation dose was small, we can assume the distribution of Frank loop was isotropic. Thus, we simply calculated the total number density of Frank loops from relrod images by using a multiplier of “4×”.

The number density and average size of dislocation loops formed in 350 °C to 5 dpa irradiation is shown in Figure 4. In Figure 4(a), for all three compositions, the number density of loops observed in dark-field images was slightly higher than that in relrod images. It may indicate the formation of perfect loops, but other possibilities also need to be considered. As discussed in our previous work [23], the easier identification of tiny loops in dark-field images than in relrod images may also contribute to a slightly higher density of loops in dark-field images. This possibility was consistent with Figure 4(b), in which the average diameter of loops in dark-field images seemed to be similar to or slightly smaller than in relrod images. Nevertheless, even if loop unfaulting occurred at 350 °C, the number density of perfect loops was low.

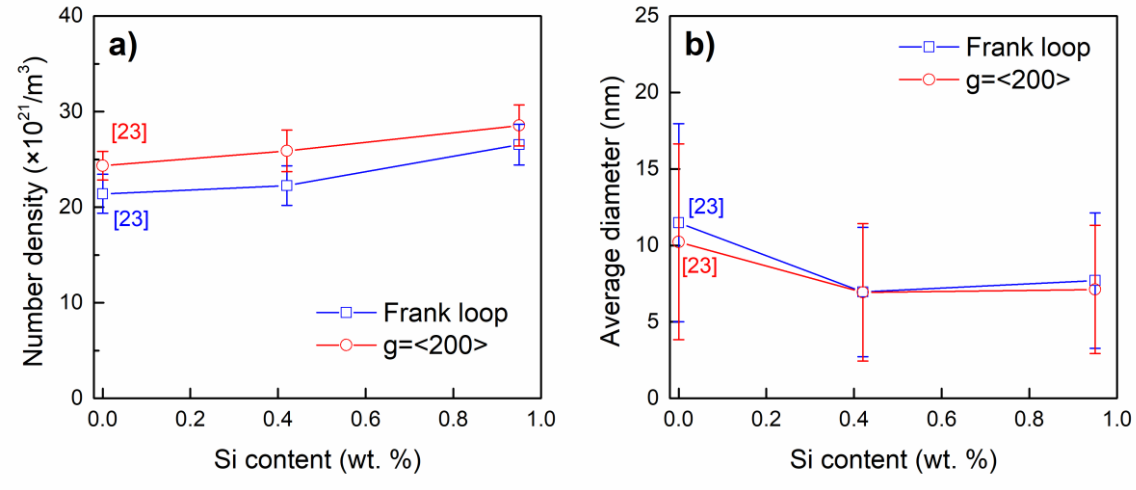

Figure 4. a) Number density and b) average size of dislocation loops in 800–1000 nm depth region observed in 350 °C and 5 dpa irradiation. Our previous results of non-Si specimen were also plotted for comparison [23].

In Figure 4, loop density slightly increased as the Si content increased, while the average size of the BA and HS specimens was distinctively smaller than the non-Si specimen. In 400 °C and 3 dpa

irradiation [24], the addition of Si was found to suppress the number density and the average size of loops, which seemed to conflict with the trend in Figure 4(a). This may be attributed to the saturation of loop number density at 5 dpa due to the limited space for microstructure evolution. In other words, as irradiation dose increased, it was possible that the non-Si alloy first reached saturation while the BA and HS still had an increase in loop density. And since the loop size was smaller in the BA and the HS specimens, the saturated loop density could be higher in those two alloys.

The dislocation loops formed in 450 °C and 5 dpa irradiation was more complicated, as shown in Figure 5. Since the number density of tiny loops was minor at the high temperature of 450 °C, the significant difference in loop number density between relrod and dark-field images was mainly caused by unfaulting, not by the easier identification of tiny loops in dark-field images. The number density of perfect loops was calculated in Figure 5(a) as a reference.

The total number density of dislocation loops (Frank loops + perfect loops) was similar between the three alloys, indicating the saturation of loop evolution. The addition of Si leaded to a higher number density of Frank loops and a lower number density of perfect loops. Therefore, the Si addition hindered the unfaulting process of Frank loops. The loop average size observed under dark-field images was larger than that under relrod images, indicating that perfect loops were larger than Frank loops in average. The addition of Si slightly reduced the size of Frank loops. The suppression effects of Si on Frank loop size were also observed in Figure 4(b), similar to the case of 400 °C and 3 dpa irradiation [24].

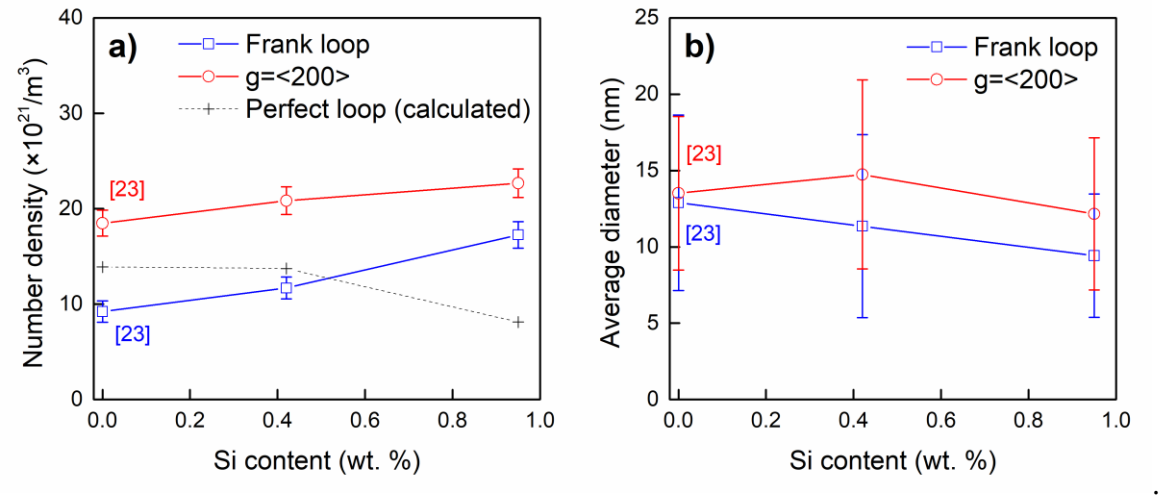

Figure 5. a) Number density and b) average size of dislocation loops in 800–1000 nm depth region observed in 450 °C and 5 dpa irradiation. Our previous results of non-Si specimen were also plotted for comparison [23].

As we know, the irradiation hardening tested by nano-indentation is linear to the tensile strength [29, 30], which depends on the square root of $N_k \times d_k$ based on the Orowan model [8]. Here N_k and d_k are the number density and average size of micro-defect type k, respectively. Since the hardening coefficient of perfect loops is lower than Frank loops [9], and the unfaulting was not obvious in 350 °C and 5 dpa irradiation, only the contribution of Frank loops to hardening is discussed. From Si content 0% to 0.42 wt.%, the size of Frank loops had an obvious drop whereas the change in the number density was small (Figure 4), which could explain the hardening decrease in Figure 3. From Si content 0.42 wt.% to 0.95 wt.%, the number density of Frank loops increased and the hardening rose again.

In the case of 450 °C and 5 dpa irradiation, multiple types of radiation defects need to be considered. In Figure 5, the HS specimen had a relatively high number density and small size of Frank loops, and the contribution of Frank loops to hardening in the HS specimen was similar or slightly higher than the other two alloys. On the other hand, the contribution of perfect loops to hardening was

low in the HS specimen due to the low number density of perfect loops. To explain the higher irradiation hardening of the HS in Figure 3, the contribution of Ni-Si clusters is essential, which were observed by atom probe tomography in our previous work using the same alloy [31]. Furthermore, the hardening coefficient of dislocation loops decorated by solute clusters [32] may be different compared to the dislocation loops without decoration.

CONCLUSION

Model alloys of stainless steel was irradiation at 350, 400, and 450 °C to 5 dpa by 3 MeV Ni^{2+}. The extent of irradiation hardening was analyzed and compared with the corresponding micro-defects. The major findings were:

1. For both the BA and the HS specimens, irradiation hardening was smaller at 400 °C compared to 350 °C and 450 °C when irradiated to 5 dpa.
2. When irradiated at the same temperature to 5 dpa, the extent of hardening was higher in the HS specimens than in the BA specimens.
3. Loop unfaulting barely occurred at 350 °C, and Frank loops were the major contributor to irradiation hardening. As Si content increased, irradiation hardening first decreased due to the suppression effects of Si on Frank loop size, and then increased as the number density of Frank loops rose.
4. Loop unfaulting was obvious at 450 °C. It was found that irradiation hardening could not be fully explained by the number density and size of loops, and the contribution of Ni-Si clusters needs to be included.

REFERENCES

[1] IAEA, Assessment and Management of Ageing of Major Nuclear Power Plant Components Important to Safety: PWR Vessel Internals, Vienna, 2007.
[2] T.S. Byun, K. Farrell, E.H. Lee, L.K. Mansur, S.A. Maloy, M.R. James, W.R. Johnson, Temperature effects on the mechanical properties of candidate SNS target container materials after proton and neutron irradiation, J Nucl Mater 303(1) (2002) 34-43.
[3] E. Wakai, S. Takaya, Y. Matsui, Y. Nagae, S. Kato, T. Suzudo, M. Yamaguchi, K. Aoto, S. Nogami, A. Hasegawa, H. Abe, K. Sato, T. Ishida, S. Makimura, P.G. Hurh, K. Ammigan, D.J. Senor, A.M. Casellal, D.J. Edwards, Irradiation damages of structural materials under different irradiation environments, J Nucl Mater 543 (2021).
[4] G.S. Was, D. Petti, S. Ukai, S. Zinkle, Materials for future nuclear energy systems, J Nucl Mater 527 (2019).
[5] JANSI, Inspection and Evaluation Guidelines for PWR Reactor Vessel Internals (Second edition), (2014).
[6] EPRI, Materials Reliability Program: PWR Internals Inspection and Evaluation Guidelines, (2011).
[7] K. Fukuya, Current understanding of radiation-induced degradation in light water reactor structural materials, J Nucl Sci Technol 50(3) (2013) 213-254.
[8] K. Fukuya, K. Fujii, H. Nishioka, Y. Kitsunai, Evolution of microstructure and microchemistry in cold-worked 316 stainless steels under PWR irradiation, J Nucl Sci Technol 43(2) (2006) 159-173.
[9] G.E. Lucas, The Evolution of Mechanical Property Change in Irradiated Austenitic Stainless-Steels, J Nucl Mater 206(2-3) (1993) 287-305.
[10] P.J. Maziasz, C.J. Mchargue, Microstructural Evolution in Annealed Austenitic Steels during Neutron-Irradiation, Int Mater Rev 32(4) (1987) 190-219.
[11] P.J. Maziasz, Overview of Microstructural Evolution in Neutron-Irradiated Austenitic Stainless-Steels, J Nucl Mater 205 (1993) 118-145.
[12] S.G. Song, J.I. Cole, S.M. Bruemmer, Formation of partial dislocations during intersection of glide dislocations with Frank loops in fcc lattices, Acta Mater 45(2) (1997) 501-511.
[13] N. Shigenaka, T. Hashimoto, M. Fuse, Effects of Alloying Elements (Mo, Si) in an Austenitic Stainless-Steel on Dislocation Loop Nucleation under Ion Irradiation, J Nucl Mater 207 (1993) 46-52.

[14] K. Fukuya, S. Nakahigashi, S. Ozaki, S. Shima, Effects of Phosphorus, Silicon and Sulfur on Microstructural Evolution in Austenitic Stainless-Steels during Electron-Irradiation, J Nucl Mater 179 (1991) 1057-1060.
[15] Y. Miwa, T. Tsukada, S. Jitsukawa, S. Kita, S. Hamada, Y. Matsui, M. Shindo, Effect of minor elements on irradiation assisted stress corrosion cracking of model austenitic stainless steels, J Nucl Mater 233 (1996) 1393-1396.
[16] J.F. Ziegler, http://www.srim.org/.
[17] K. Fujii, K. Fukuya, Effects of radiation on spinodal decomposition of ferrite in duplex stainless steel, J Nucl Mater 440(1-3) (2013) 612-616.
[18] J.T. Busby, M.M. Sowa, G.S. Was, E.P. Simonen, Post-irradiation annealing of small defect clusters, Philos Mag 85(4-7) (2005) 609-617.
[19] A. Lupinacci, K. Chen, Y. Li, M. Kunz, Z. Jiao, G.S. Was, M.D. Abad, A.M. Minor, P. Hosemann, Characterization of ion beam irradiated 304 stainless steel utilizing nanoindentation and Laue microdiffraction, J Nucl Mater 458 (2015) 70-76.
[20] T. Miura, K. Fujii, K. Fukuya, K. Takashima, Influence of crystal orientation on hardness and nanoindentation deformation in ion-irradiated stainless steels, J Nucl Mater 417(1-3) (2011) 984-987.
[21] D.J. Edwards, E.P. Simonen, S.M. Bruemmer, Evolution of fine-scale defects in stainless steels neutron-irradiated at 275 degrees C, J Nucl Mater 317(1) (2003) 13-31.
[22] P.J. Barton, B.L. Eyre, D.A. Stow, Structure of Fast-Reactor Irradiated Solution-Treated Aisi Type-316 Steel, J Nucl Mater 67(1-2) (1977) 181-197.
[23] D.Y. Chen, K. Murakami, K. Dohi, K. Nishida, Z.C. Li, N. Sekimura, The effects of loop size on the unfaulting of Frank loops in heavy ion irradiation, J Nucl Mater 529 (2020).
[24] D.Y. Chen, K. Murakami, K. Dohi, K. Nishida, N. Soneda, Z.C. Li, L. Liu, N. Sekimura, Depth distribution of Frank loop defects formed in ion-irradiated stainless steel and its dependence on Si addition, Nucl Instrum Meth B 365 (2015) 503-508.
[25] D.Y. Chen, K. Murakami, K. Dohi, K. Nishida, N. Soneda, Z.C. Li, L. Liu, N. Sekimura, Radiation Defects Formed in Ion-Irradiated 316L Stainless Steel Model Alloys with Different Si Additions, Mater Trans 56(9) (2015) 1549-1552.
[26] K.I. Fukumoto, T. Mabuchi, K. Yabuuchi, K. Fujii, Irradiation hardening of stainless steel model alloy after Fe-ion irradiation and post-irradiation annealing treatment, J Nucl Mater 557 (2021).
[27] H.R. Brager, F.A. Garner, G.L. Guthrie, Effect of Stress on Microstructure of Neutron-Irradiated Type-316 Stainless-Steel, J Nucl Mater 66(3) (1977) 301-321.
[28] X. Liu, J.G. Gigax, J.D. Poplawsky, W. Guo, H. Kim, L. Shao, F.A. Garner, J.F. Stubbins, Radiation response of a Fe-20Cr-25Ni austenitic stainless steel under Fe2+ irradiation at 500 degrees C, Materialia 9 (2020).
[29] J.T. Busby, M.C. Hash, G.S. Was, The relationship between hardness and yield stress in irradiated austenitic and ferritic steels, J Nucl Mater 336(2-3) (2005) 267-278.
[30] K. Yabuuchi, Y. Kuribayashi, S. Nogami, R. Kasada, A. Hasegawa, Evaluation of irradiation hardening of proton irradiated stainless steels by nanoindentation, J Nucl Mater 446(1-3) (2014) 142-147.
[31] D.Y. Chen, K. Murakami, K. Dohi, K. Nishida, L. Chen, Z.C. Li, N. Sekimura, Formation of Ni-Si clusters and their relationship with dislocation loops in irradiated stainless steels, J Nucl Mater 578 (2023) 154366.
[32] M. Song, K.G. Field, R.M. Cox, G.S. Was, Microstructural characterization of cold-worked 316 stainless steel flux thimble tubes irradiated up to 100 dpa in a commercial Pressurized Water Reactor, J Nucl Mater 541 (2020).